

*This copy is for your personal, non-commercial use only.*

**If you wish to distribute this article to others**, you can order high-quality copies for your colleagues, clients, or customers by [clicking here](#).

**Permission to republish or repurpose articles or portions of articles** can be obtained by following the guidelines [here](#).

***The following resources related to this article are available online at [www.sciencemag.org](http://www.sciencemag.org) (this information is current as of October 19, 2010):***

**Updated information and services**, including high-resolution figures, can be found in the online version of this article at:

<http://www.sciencemag.org/cgi/content/full/283/5402/663>

This article has been **cited by** 265 article(s) on the ISI Web of Science.

This article appears in the following **subject collections**:

Physics, Applied

[http://www.sciencemag.org/cgi/collection/app\\_physics](http://www.sciencemag.org/cgi/collection/app_physics)

are transported from the tip to the substrate. Although the experiments performed on Au(111)/mica provide important information about the chemical identity of the transported species in these experiments, Au(111)/mica is a poor substrate for DPN. The deep valleys around the small Au(111) facets make it difficult to draw long (micrometer) contiguous lines with nanometer widths.

Although the nonannealed Au substrates are relatively rough (the root mean square roughness is 2 nm), we could deposit 30-nm lines with DPN; this distance is the average Au grain diameter of our thin film substrates and represents the resolution limit of DPN on this type of substrate (Fig. 2C). The 30-nm molecule-based line prepared on this type of substrate is discontinuous and follows the grain edges of the Au. Smoother and more contiguous lines can be drawn by increasing the line width to 100 nm (Fig. 2D) or presumably by using a smoother Au substrate. The width of the line depends on tip scan speed and the rate of transport of the alkanethiol from the tip to the substrate (relative humidity can change the transport rate). Faster scan speeds and a smaller number of traces give narrower lines.

We also used DPN to prepare molecular dot features to demonstrate the diffusion properties of the "ink" (Fig. 3, A and B). The ODT-coated tip was brought into contact (set point = 1 nN) with the Au substrate for a set period of time. For example, ODT dots 0.66  $\mu\text{m}$ , 0.88  $\mu\text{m}$ , and 1.6  $\mu\text{m}$  in diameter were generated by holding the tip in contact with the surface for 2, 4, and 16 min, respectively (Fig. 3A, left to right). The uniform appearance of the dots probably reflects an even flow of ODT in all directions from the tip to the surface. Opposite contrast images were obtained by depositing dots of an alkanethiol derivative, 16-mercaptohexadecanoic acid, in an analogous fashion (Fig. 3B). This not only provides additional evidence that the molecules are being transported from the tip to the surface but also demonstrates the molecular generality of DPN.

We could generate arrays and grids in addition to individual lines and dots. An array of 25 ODT dots 0.46  $\mu\text{m}$  in diameter, spaced 0.54  $\mu\text{m}$  apart (Fig. 3C), was generated by holding an ODT-coated tip in contact with the surface (1 nN) for 20 s at 45% relative humidity without lateral movement to form each dot. A grid consisting of eight intersecting lines 2  $\mu\text{m}$  in length and 100 nm wide (Fig. 3D) was generated by sweeping the ODT-coated tip on a Au surface at a 4- $\mu\text{m}/\text{s}$  scan speed with a 1-nN force for 1.5 min to form each line.

The resolution of DPN depends on several parameters, and its ultimate resolution is not yet clear. First, the grain size of the substrate affects DPN resolution much as the texture of paper controls the resolution of conventional writing. Second, chemisorption and self assembly can be used to limit the diffusion of the molecules

after deposition. The ODT patterns are stable whereas water forms metastable patterns (23). Third, the tip-substrate contact time and thus the scan speed influence DPN resolution. Fourth, relative humidity seems to affect the resolution of the lithographic process by controlling the rate of ODT transport from the tip to the substrate. The size of the water meniscus that bridges the tip and substrate depends on relative humidity (23). For example, the 30-nm-wide line (Fig. 1C) required 5 min to generate in a 34% relative humidity environment, whereas the 100-nm line (Fig. 1D) required 1.5 min to generate in a 42% relative humidity environment.

DPN is a simple but powerful method for transporting molecules from AFM tips to substrates at resolutions comparable to those achieved with much more expensive and sophisticated competitive lithographic methods, such as electron-beam lithography. It should be especially useful for the detailed functionalization of nanoscale devices prepared by more conventional lithographic methods (30, 31).

References and Notes

1. A. C. Ewing, *The Fountain Pen: A Collector's Companion* (Running Press, Philadelphia, PA, 1997).
2. Y. Xia and G. M. Whitesides, *Angew. Chem. Int. Ed. Engl.* **37**, 550 (1998).
3. E. Kim, Y. Xia, G. M. Whitesides, *Nature* **376**, 581 (1995).
4. Y. Xia et al., *Science* **273**, 347 (1996).
5. L. Yan, X.-M. Zhao, G. M. Whitesides, *J. Am. Chem. Soc.* **120**, 6179 (1998).
6. A. Kumar, H. A. Biebuyck, N. L. Abbott, G. M. Whitesides, *ibid.* **114**, 9188 (1992).
7. L. A. Bottomley, *Anal. Chem.* **70**, 425R (1998).
8. R. M. Nyffenegger and R. M. Penner, *Chem. Rev.* **97**, 1195 (1997).

9. K. K. Berggren et al., *Science* **269**, 1255 (1995).
10. J. A. M. Sondag-Huethorst, H. R. J. van Helleputte, L. G. J. Fokkink, *Appl. Phys. Lett.* **64**, 285 (1994).
11. J. K. Schoer and R. M. Crooks, *Langmuir* **13**, 2323 (1997).
12. S. Xu and G. Liu, *ibid.*, p. 127.
13. F. K. Perkins et al., *Appl. Phys. Lett.* **68**, 550 (1996).
14. D. W. Carr et al., *J. Vac. Sci. Technol. A* **15**, 1446 (1997).
15. M. J. Lercel, H. G. Craighead, A. N. Parikh, K. Seshadri, D. L. Allara, *Appl. Phys. Lett.* **68**, 1504 (1996).
16. H. Sugimura and N. Nakagiri, *J. Vac. Sci. Technol. A* **14**, 1223 (1996).
17. T. Komeda, K. Namba, Y. Nishioka, *ibid.* **16**, 1680 (1998).
18. H. U. Muller, C. David, B. Volkel, M. Grunze, *J. Vac. Sci. Technol. B* **13**, 2846 (1995).
19. Y. Kim and C. M. Lieber, *Science* **257**, 375 (1992).
20. L. Xu, A. Lio, J. Hu, D. F. Ogletree, M. Salmeron, *J. Phys. Chem. B* **102**, 540 (1998).
21. M. Binggeli and C. M. Mate, *Appl. Phys. Lett.* **65**, 415 (1994).
22. M. Fujihira et al., *Chem. Lett.* (1996), p. 499.
23. R. D. Piner and C. A. Mirkin, *Langmuir* **13**, 6864 (1997).
24. C. D. Bain and G. M. Whitesides, *Angew. Chem. Int. Ed. Engl.* **28**, 506 (1989).
25. A. Ulman, *An Introduction to Ultrathin Organic Films: From Langmuir-Blodgett to Self-Assembly* (Academic Press, Boston, MA, 1991).
26. L. H. Dubois and R. G. Nuzzo, *Annu. Rev. Phys. Chem.* **43**, 437 (1992).
27. A. R. Bishop and R. G. Nuzzo, *Curr. Opin. Coll. Interf. Sci.* **1**, 127 (1996).
28. C. A. Alves, E. L. Smith, M. D. Porter, *J. Am. Chem. Soc.* **114**, 1222 (1992).
29. A Park Scientific Model CP instrument was used to perform all experiments. The scanner was enclosed in a glass isolation chamber, and the relative humidity was measured with a hygrometer. All humidity measurements have an absolute error of  $\pm 5\%$ .
30. M. A. Reed, C. Zhou, C. J. Muller, T. P. Burgin, J. M. Tour, *Science* **278**, 252 (1997).
31. D. L. Feldheim and C. D. Keating, *Chem. Soc. Rev.* **27**, 1 (1998).
32. C.A.M. acknowledges the Air Force Office of Scientific Research and the NSF-funded Northwestern University Materials Research Center for support of this work.

24 September 1998; accepted 22 December 1998

## Visible Quantum Cutting in LiGdF<sub>4</sub>:Eu<sup>3+</sup> Through Downconversion

René T. Wegh, Harry Donker, Koenraad D. Oskam, Andries Meijerink\*

For mercury-free fluorescent lamps and plasma display panels, alternative luminescent materials are required for the efficient conversion of vacuum ultraviolet radiation to visible light. Quantum cutting involving the emission of two visible photons for each vacuum ultraviolet photon absorbed is demonstrated in Eu<sup>3+</sup>-doped LiGdF<sub>4</sub> with the concept of downconversion. Upon excitation of Gd<sup>3+</sup> with a high-energy photon, two visible photons can be emitted by Eu<sup>3+</sup> through an efficient two-step energy transfer from Gd<sup>3+</sup> to Eu<sup>3+</sup>, with a quantum efficiency that approaches 200 percent.

Luminescent materials with lanthanides are found in fluorescent tubes, color televisions, x-ray photography, lasers, infrared (IR) to visible light upconversion materials, and fiber amplifiers (1-3). Such applications rely

on the luminescence properties of lanthanide ions (sharp lines and high efficiency). In fluorescent lamps, phosphors on the inside wall of the glass tube convert the ultraviolet (UV) radiation (mainly with a wavelength  $\lambda$  of 254

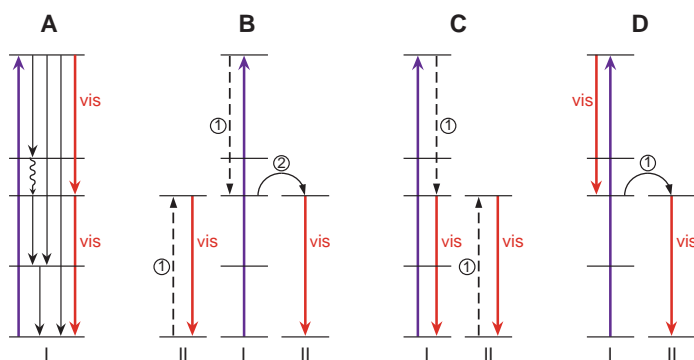
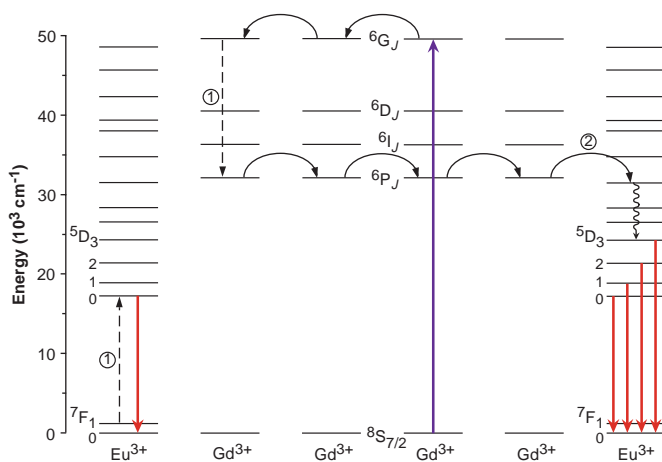


**Fig. 1 (left).** Energy level diagrams for two (hypothetical) types of lanthanide ions (I and II), showing the concept of downconversion. Type I is an ion for which emission from a high energy level can occur. Type II is an ion to which energy transfer takes place. **(A)** Quantum cutting on a single ion I by the sequential emission of two visible photons. **(B)** The possibility of quantum cutting by a two-step energy transfer. In the first step (indicated by ①), a part of the excitation energy is transferred from ion I to ion II by cross-relaxation. Ion II returns to the ground state by emitting one photon of visible light. Ion I is still in an excited state and can transfer the remaining energy to a second ion of type II (indicated by ②), which also emits a photon



in the visible spectral region, giving a quantum efficiency of 200%. **(C and D)** The remaining two possibilities involve only one energy transfer step from ion I to ion II. This is sufficient to obtain visible quantum cutting if one of the two visible photons can be emitted by ion I. **Fig. 2 (right).** Energy level diagram of the  $Gd^{3+}$ - $Eu^{3+}$  system, showing the possibility of visible quantum cutting by a two-step energy transfer from  $Gd^{3+}$  to  $Eu^{3+}$ .

nm) that is generated in the Hg discharge to blue, green, and red light, yielding white light. The quantum efficiency of the lanthanide-based lamp phosphors is high (~90%) (1): For every 100 UV photons that are absorbed, 90 photons in the visible spectral region are emitted.

A challenge in the field of luminescence of lanthanide ions is the research in the vacuum ultraviolet (VUV) ( $\lambda < 200$  nm) spectral region. Recently, this field has become important because of the need for phosphors for VUV excitation (1, 3–5). For example, Hg-free fluorescent lamps can be made by replacing Hg with a noble gas, such as Xe, as the discharge medium. A Xe discharge offers the advantage of immediate start-up: There is no delay in the emission of light (as is the case in conventional fluorescent lamps, where Hg must first evaporate). Immediate start-up is important in special applications (for example, for lamps in facsimile and copying machines and for car brake lights. In plasma display panels, a Xe discharge is also used to generate VUV radiation. In each pixel, the VUV radiation is converted to blue, green, or red light by a phosphor (4). For the conversion of the VUV radiation of a Xe discharge ( $\lambda \approx 172$  nm) to visible light, alternative phosphors are needed. Three aspects are important in the development of new VUV phosphors: a higher efficiency, a higher stability, and a higher VUV absorption (5).

Although the generation efficiency of VUV radiation is high in a Xe discharge (higher than in other noble gas discharges), the light output (in lumens per watt) of Xe-

discharge lamps is lower than that of Hg-based fluorescent lamps. An important limitation in obtaining high energy efficiencies is inherent to the conversion of one VUV photon ( $\lambda \approx 172$  nm) to one visible photon ( $\lambda = 400$  to  $700$  nm). Even if the quantum efficiency of a phosphor is 100%, in this process, ~65% of the energy from the VUV photon is lost by nonradiative relaxation processes. For a Hg discharge ( $\lambda = 254$  nm), the losses are lower (~50%). To reduce the higher energy losses, a quantum efficiency of more than 100% is required for phosphors in Xe-discharge fluorescent lamps. In theory, this is possible as the high energy of VUV photons that are generated in a noble gas discharge allows the emission of two photons in the visible spectral region per each VUV photon absorbed. This phenomenon has been studied for single lanthanide ions like  $Pr^{3+}$  and  $Tm^{3+}$  (6, 7), but for  $Tm^{3+}$ , a substantial amount of light is lost in the IR or UV spectral region,

whereas for  $Pr^{3+}$ , the main emission occurs in the deep violet region (~405 nm), where eye sensitivity is very low.

An alternative concept for obtaining quantum efficiencies of more than 100% is based on a combination of two lanthanide ions. Through partial energy transfer between the ions, a high quantum efficiency (close to 200%) can be obtained. This process is the opposite of the process that is known as “Addition de Photons par Transfert d’Energie” (APTE) [which was discovered by Auzel in 1966 (8)] and also known as upconversion (1, 2). Because of this analogy, we call the quantum cutting through energy transfer “downconversion.” The concept is illustrated (Fig. 1) with two types of ions, I and II, with hypothetical energy level schemes. Efficient visible quantum cutting by a two-photon emission from a high energy level for a single lanthanide ion is theoretically possible (Fig. 1A, red lines). However,

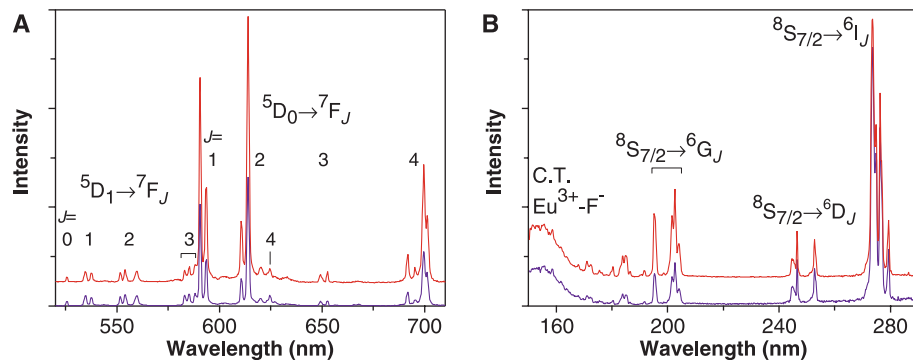


**Fig. 3. (A)** Emission spectra of  $LiGdF_4:Eu^{3+}$  (0.5 mol%) upon excitation in the  $6I_1$  levels of  $Gd^{3+}$  at 273 nm (violet line) and upon excitation in the  $6G_J$  levels of  $Gd^{3+}$  at 202 nm (red line), both at 300 K. The spectra are scaled on the  $5D_1 \rightarrow 7F_J$  emission intensity. **(B)** Excitation spectra of  $LiGdF_4:Eu^{3+}$  (0.5 mol%) monitoring the  $5D_1 \rightarrow 7F_2$  emission of  $Eu^{3+}$  at 554 nm (violet line) and the  $5D_0 \rightarrow 7F_2$  emission at 614 nm (red line), both at 300 K. The spectra are scaled on the  $8S_{7/2} \rightarrow 6I_1$  excitation intensity.

Debye Institute, Utrecht University, Post Office Box 80 000, 3508 TA Utrecht, Netherlands.

\*To whom correspondence should be addressed. E-mail: a.meijerink@phys.uu.nl

competing emissions in the IR and UV regions (Fig. 1A, black lines) can also occur. Possibilities for visible quantum cutting involving the known energy levels of lanthanides (up to 50,000 cm<sup>-1</sup>) have been studied with the Judd-Ofelt theory, but efficient visible quantum cutting by the sequential emission of two visible photons on one lanthanide ion has not been found (3, 7). The use of a second type of lanthanide ion, to which a part of the excitation energy can be transferred and which subsequently emits a visible photon, can prevent losses in the IR and UV regions. There are three possibilities for visible quantum cutting through energy transfer (Fig. 1, B through D), all of which have a theoretical quantum efficiency of 200%.

The emission of two visible photons per each absorbed VUV photon is possible with the Gd<sup>3+</sup>-Eu<sup>3+</sup> couple (Fig. 2). We have observed visible emission from Gd<sup>3+</sup> at ~590 nm upon excitation in the <sup>6</sup>G<sub>J</sub> levels at ~50,000 cm<sup>-1</sup> (9); *J* is the total angular momentum quantum number. The emission could be assigned to the <sup>6</sup>G<sub>J</sub> → <sup>6</sup>P<sub>7/2</sub> transition. The energy of this emission matches the <sup>7</sup>F<sub>J</sub> → <sup>5</sup>D<sub>0</sub> excitation energy on Eu<sup>3+</sup>. Visible quantum cutting of the type indicated in Fig. 1B can now occur. Upon excitation in the <sup>6</sup>G<sub>J</sub> levels of Gd<sup>3+</sup>, energy is transferred in the first step by cross-relaxation between Gd<sup>3+</sup> in the <sup>6</sup>G<sub>J</sub> state and Eu<sup>3+</sup> in the <sup>7</sup>F<sub>J</sub> state, resulting in Gd<sup>3+</sup> in the <sup>6</sup>P<sub>J</sub> state and Eu<sup>3+</sup> in the <sup>5</sup>D<sub>0</sub> state. In the second step, the Gd<sup>3+</sup> ion in the <sup>6</sup>P<sub>J</sub> state transfers the remaining excitation energy to a high excited state of a second Eu<sup>3+</sup> ion. Fast relaxation from this high excited state to the <sup>5</sup>D<sub>J</sub> states occurs. Both steps result in the emission of a visible photon due to <sup>5</sup>D<sub>J</sub> → <sup>7</sup>F<sub>J</sub> transitions on Eu<sup>3+</sup>, where the energy transfer from Gd<sup>3+</sup> to Eu<sup>3+</sup> is mediated by energy migration over the excited states of the Gd<sup>3+</sup> ions. Energy migration over the Gd sublattice in concentrated Gd compounds is well known and allows an efficient energy transfer with low Eu concentrations, because the Eu<sup>3+</sup> ions act as traps for the excitation energy migrating over the Gd sublattice (1, 2).

To investigate if and with what efficiency the visible quantum cutting in the Gd<sup>3+</sup>-Eu<sup>3+</sup> system occurs, we synthesized polycrystalline powder samples of LiGdF<sub>4</sub>:Eu<sup>3+</sup> [0.5 mole percent (mol%)] (9). Extreme care was taken to prevent contamination of the samples with oxygen. The luminescence measurements were performed on set-ups, which are described in detail in (9). In determining the efficiency of the quantum cutting process, it may seem straightforward to measure the quantum efficiency of the phosphor under VUV excitation. This method has two drawbacks. First, it is difficult to determine the quantum efficiency of a weakly absorbing phosphor. Because the excitation transitions on the Gd<sup>3+</sup> ion are parity-forbidden transitions within the 4f<sup>7</sup> configuration, the

VUV absorption is weak, and the error in the determination of the fraction of the VUV radiation that is absorbed is large. This gives a large error in the quantum efficiency calculated. The second problem is related to other processes that can influence the quantum efficiency, especially in a phosphor that has not been optimized. Nonradiative losses at defects and impurities can lower the quantum efficiency, and even if the two-step energy transfer process occurs with high efficiency, a quantum efficiency that is much lower than 200% is measured. An optimized phosphor could still have a quantum efficiency close to 200%.

It is possible to determine the efficiency of the two-step energy transfer process (emitting two photons in the visible spectral region) relative to the process that emits only one visible photon (direct energy transfer from the <sup>6</sup>G<sub>J</sub> level of Gd<sup>3+</sup> to a Eu<sup>3+</sup> level at ~50,000 cm<sup>-1</sup>). In the emission spectra, the intensity distribution over the different Eu<sup>3+</sup> emission lines depends on the energy transfer process. The percentage of the Gd<sup>3+</sup> ions that relax through a two-step energy transfer to Eu<sup>3+</sup> can be determined from changes in the ratio of the intensity of the <sup>5</sup>D<sub>0</sub> emission and the other <sup>5</sup>D<sub>J</sub> emissions for different excitation wavelengths. The emission spectrum (Fig. 3A, violet line) shows that the emission lines corresponding to transitions from the <sup>5</sup>D<sub>0</sub> level are the strongest, but emission from the <sup>5</sup>D<sub>1</sub> levels was also observed. Weak emission lines from the <sup>5</sup>D<sub>2</sub> and the <sup>5</sup>D<sub>3</sub> levels were observed but not shown (10). The emission spectrum is in good agreement with spectra for Eu<sup>3+</sup> in LiYF<sub>4</sub> and LiGdF<sub>4</sub> (11). The ratio of the intensities of the <sup>5</sup>D<sub>0</sub>, <sup>5</sup>D<sub>1</sub>, <sup>5</sup>D<sub>2</sub>, and <sup>5</sup>D<sub>3</sub> emission lines (the branching ratio) is the same for excitation in a high Eu<sup>3+</sup> level (above the <sup>5</sup>D<sub>3</sub> level) or after direct energy transfer from Gd<sup>3+</sup> to Eu<sup>3+</sup>. This branching ratio, determined by competition between multiphonon relaxation and radiative decay from the <sup>5</sup>D<sub>J</sub> levels, is called the “normal” branching ratio.

Upon excitation in the <sup>6</sup>G<sub>J</sub> level, quantum cutting through a two-step energy transfer can occur. In the first step of this process, only the <sup>5</sup>D<sub>0</sub> level of Eu<sup>3+</sup> is excited (Fig. 2). In the second step, energy is transferred from the <sup>6</sup>P level of Gd<sup>3+</sup> to a high energy level of Eu<sup>3+</sup>. This second step yields the normal branching ratio for the different <sup>5</sup>D<sub>J</sub> emission lines. As the first energy transfer step only gives the emission from the <sup>5</sup>D<sub>0</sub> level of Eu<sup>3+</sup>, a substantial increase of the relative intensity of the <sup>5</sup>D<sub>0</sub> emission intensity upon excitation in the <sup>6</sup>G<sub>J</sub> levels is expected, if quantum cutting through a two-step energy transfer occurs as indicated in Fig. 2. A comparison of the emission spectra for excitation in the <sup>6</sup>I<sub>J</sub> levels of Gd<sup>3+</sup> (273 nm) (Fig. 3A, violet line) and in the <sup>6</sup>G<sub>J</sub> levels of Gd<sup>3+</sup> (202 nm) (Fig. 3A, red line) shows that the relative intensity of the <sup>5</sup>D<sub>0</sub> emission lines is indeed more than a factor of 2 stronger for

excitation in the <sup>6</sup>G<sub>J</sub> levels than for excitation in the <sup>6</sup>I<sub>J</sub> levels. The <sup>5</sup>D<sub>0</sub>/<sup>5</sup>D<sub>1,2,3</sub> emission intensity ratio is 3.4 for excitation in the <sup>6</sup>I<sub>J</sub> levels (this is the normal branching ratio). Upon excitation in the <sup>6</sup>G<sub>J</sub> levels of Gd<sup>3+</sup> (or in other Gd<sup>3+</sup> levels in the VUV), the <sup>5</sup>D<sub>0</sub>/<sup>5</sup>D<sub>1,2,3</sub> emission intensity ratio is 7.4. From these intensity ratios, the efficiency of the cross-relaxation step can be determined with

$$\frac{P_{CR}}{P_{CR} + P_{DT}} = \frac{R(^5D_0/^5D_{1,2,3})_{G_j} - R(^5D_0/^5D_{1,2,3})_{I_j}}{R(^5D_0/^5D_{1,2,3})_{I_j} + 1}$$

Here, *P*<sub>CR</sub> is the probability for cross-relaxation, and *P*<sub>DT</sub> is the probability for the direct energy transfer from Gd<sup>3+</sup> to Eu<sup>3+</sup>. *R*(<sup>5</sup>D<sub>0</sub>/<sup>5</sup>D<sub>1,2,3</sub>) is the ratio of the <sup>5</sup>D<sub>0</sub> and the <sup>5</sup>D<sub>1,2,3</sub> emission intensities. The subscript (<sup>6</sup>G<sub>J</sub> or <sup>6</sup>I<sub>J</sub>) indicates the excitation level for which the ratio is obtained. From the *R*(<sup>5</sup>D<sub>0</sub>/<sup>5</sup>D<sub>1,2,3</sub>) values of 3.4 (for <sup>6</sup>I<sub>J</sub> excitation) and 7.4 (for <sup>6</sup>G<sub>J</sub> excitation), the ratio *P*<sub>CR</sub>/(*P*<sub>CR</sub> + *P*<sub>DT</sub>) was calculated to be ~0.9, showing that 9 of 10 Gd<sup>3+</sup> ions in the <sup>6</sup>G<sub>J</sub> excited state relax through a two-step energy transfer to Eu<sup>3+</sup>, yielding two visible photons. One of 10 Gd<sup>3+</sup> ions in the excited <sup>6</sup>G<sub>J</sub> state transfers all its energy directly to a high energy level of Eu<sup>3+</sup>, resulting in the emission of only one visible photon. In this way, a visible quantum efficiency of 190% can be obtained if nonradiative losses (for example, losses due to energy migration and energy transfer to nonradiative quenching centers in the lattice) can be prevented. Experience with lanthanide phosphors has shown that nonradiative losses can be low if the synthesis procedure is optimized. Thus, in an optimized LiGdF<sub>4</sub>:Eu<sup>3+</sup> phosphor, a quantum efficiency close to 200% may be possible. Losses due to UV emission from Gd<sup>3+</sup> are negligible; in the emission spectra, only very weak Gd<sup>3+</sup> emission lines were observed. The intensity of these lines was much less than 1% of the total emission intensity, which shows that the energy transfer from Gd<sup>3+</sup> to Eu<sup>3+</sup> through energy migration is efficient.

In the excitation spectra of two Eu<sup>3+</sup> emission lines, the relative intensity of Gd<sup>3+</sup> excitation lines corresponding to transitions in the VUV is more than a factor of 2 higher in the excitation spectrum of the <sup>5</sup>D<sub>0</sub> emission (Fig. 3B, red line) than in the excitation spectrum of the <sup>5</sup>D<sub>1</sub> emission (Fig. 3B, violet line). This is in agreement with the observations in the emission spectrum presented above, and it confirms the presence of quantum cutting through down-conversion. The demonstration of down-conversion in LiGdF<sub>4</sub>:Eu<sup>3+</sup> with a quantum efficiency close to 200% in the orange or red spectral region is an important step in

the development of more efficient Hg-free fluorescent tubes and plasma display panels and has triggered the search for downconversion phosphors with quantum efficiencies that are higher than 100% in the blue and green spectral regions.

References and Notes

1. G. Blasse and B. C. Grabmaier, *Luminescent Materials* (Springer-Verlag, Berlin, 1994).
2. B. Henderson and G. F. Imbusch, *Optical Spectroscopy in Inorganic Solids* (Clarendon, Oxford, 1989).
3. C. R. Ronda, *J. Alloys Compd.* **225**, 534 (1995).
4. S. W. Depp and W. E. Howard, *Sci. Am.* **260**, 40 (March 1993).

5. F. Vollkommer and L. Hitzschke, *Phys. Bl.* **53**, 887 (1997).
6. J. L. Sommerdijk, A. Brill, A. W. de Jager, *J. Lumin.* **8**, 341 (1974); W. W. Piper, J. A. DeLuca, F. S. Ham, *ibid.*, p. 344; A. M. Srivastava, D. A. Dougherty, W. W. Beers, *J. Electrochem. Soc.* **143**, 4113 (1996).
7. R. Pappalardo, *J. Lumin.* **14**, 159 (1976).
8. F. Auzel, *C. R. Acad. Sci. Paris* **262**, 1016 (1966).
9. R. T. Wegh, H. Donker, A. Meijerink, R. J. Lamminmäki, J. Hölsä, *Phys. Rev. B* **56**, 13841 (1997).
10. The energy gaps between the different  $^5D_j$  levels of  $\text{Eu}^{3+}$  is such that four or five phonons of the highest possible energy ( $\sim 500 \text{ cm}^{-1}$  in  $\text{LiGdF}_4$ ) are required to bridge the gap. For this situation, the radiative decay can compete with nonradiative decay to lower  $^5D_j$  levels, and emission from all  $^5D_j$  levels was observed.

11. J. P. M. van Vliet, D. van der Voort, G. Blasse, *J. Lumin.* **42**, 305 (1989); C. Görrler-Walrand, K. Binnemans, L. Fluyt, *J. Phys. Condens. Matter* **5**, 8359 (1993).
12. The authors are grateful to P. Gürtler from Hamburger Synchrotronstrahlungslabor (HASYLAB) for the opportunity to measure at the HIGITI experimental station at the Deutsches Elektronen Synchrotron (DESY) in Hamburg, Germany. The work described here was supported by the Council for Chemical Sciences (CW), with financial aid from the Netherlands Organization for Scientific Research (NWO) and the Netherlands Foundation for Technical Research (STW). Financial support from Philips Lighting is gratefully acknowledged.

29 September 1998; accepted 15 December 1998

## Argon-Lead Isotopic Correlation in Mid-Atlantic Ridge Basalts

Philippe Sarda,\* Manuel Moreira,† Thomas Staudacher‡

Step-heating analyses for Mid-Atlantic Ridge glass samples show that maximum  $^{40}\text{Ar}/^{36}\text{Ar}$  values correlate with  $^{206,207,208}\text{Pb}/^{204}\text{Pb}$ . These correlations hold for the whole Atlantic Ocean and therefore are unlikely to result from shallow-level contamination processes. Instead, they are taken as mixing hyperbolae between the degassed-depleted upper mantle and a recycled component characterized by high  $^{206}\text{Pb}/^{204}\text{Pb}$  ratios (19 to 21) and low  $^{40}\text{Ar}/^{36}\text{Ar}$  ratios (300 to 1000). These relations imply that argon may also be a tracer of mantle recycling.

Rare gas isotopes have been successfully used to constrain the timing of atmosphere generation by mantle degassing (1–5), but, except for helium (6, 7), they have been less useful as tracers of mantle heterogeneities, largely because of contamination by atmospheric rare gases (8, 9). Measuring the isotopic composition of mantle rare gases trapped in mid-ocean ridge basalt (MORB) has always met the difficulty of separating the magmatic gas from a widespread atmospheric component, a particular problem for argon. Addition of atmospheric Ar was long considered to occur during eruption on the sea floor. Indeed, the slowly cooled inner parts of submarine lava flows generally appear more contaminated than the outer layers, quenched to glass (8, 9). In step-heating degassing on glass samples, argon with  $^{40}\text{Ar}/^{36}\text{Ar}$  ratios of 300 to 5000 is often

released in the low-temperature steps (500° to 700°C). This gas is confirmation that weakly bound atmospheric argon is present in many samples (9–13).

In higher temperature steps, argon with high to very high  $^{40}\text{Ar}/^{36}\text{Ar}$  ratios of 10,000 to 30,000 is commonly released (9–13). For a given sample, the maximum value obtained in a series of temperature steps is taken as the most representative of the true magmatic value, at least a minimum value because some contaminant argon may still be present. Such high  $^{40}\text{Ar}/^{36}\text{Ar}$  ratios, and similar isotopic anomalies for the other rare gases, record the highly degassed character of the upper mantle (4, 5, 9, 11), or at least of parts of it.

Overall,  $^{40}\text{Ar}/^{36}\text{Ar}$  maxima from step-heating analyses obtained for numerous mid-ocean ridge glass samples from diverse locations worldwide display a large range of values, from 500 to about 30,000 (3, 9, 12–16). Most authors have assumed that this variability reflects the inability of the analysis techniques to separate completely magmatic argon from contaminant argon (9, 12, 14–16). If this were the case, upper-mantle argon could be isotopically uniform and have a high  $^{40}\text{Ar}/^{36}\text{Ar}$  signature. However, neither step-heating nor step-crushing of glass samples have ever demonstrated the existence of this single mantle argon component. In contrast, decades of improving analyses have shown that the variability of  $^{40}\text{Ar}/^{36}\text{Ar}$  maxima from step-heating or crushing is the rule. Therefore, there is a possibility that

this variability may be not merely due to contamination, but is at least partly inherent to mantle argon. Argon might then bear the record of some mantle heterogeneities, in the same way as Sr, Nd, or Pb.

To test this possibility, we analyzed the IGP rare gas laboratory's large argon isotopic database for MORB to determine whether any correlation could be found between  $^{40}\text{Ar}/^{36}\text{Ar}$  ratios and Pb isotope data from the literature. Initially, we used only step-heating data where more than one temperature step was performed. Samples with a  $^4\text{He}/^3\text{He}$  ratio lower than 75,000 ( $^3\text{He}/^4\text{He}$  higher than 9.5 Ra) were not used, as they are considered to be influenced by primitive plumes from the lower mantle. For every sample, the highest  $^{40}\text{Ar}/^{36}\text{Ar}$  value from the different temperature steps was retained. When replicate argon analyses were performed, only the highest value was selected. A few samples with  $^{40}\text{Ar}/^{36}\text{Ar}$  ratios lower than 1000 were discarded as possibly severely contaminated. Then, one maximum  $^{40}\text{Ar}/^{36}\text{Ar}$  ratio from step-crushing was added (and one datum from total fusion). In all, 20 analyses were identified for North and South Atlantic Ocean samples having the same identification in our database for Ar and in the literature for Pb. We also included recent data for the Azores section of the Mid-Atlantic Ridge, with radiogenic lead and  $^{40}\text{Ar}/^{36}\text{Ar}$  mostly lower than 1000, giving 28 samples (17).

The  $^{40}\text{Ar}/^{36}\text{Ar}$  ratio in these samples correlates with  $^{206}\text{Pb}/^{204}\text{Pb}$ ,  $^{207}\text{Pb}/^{204}\text{Pb}$ , and  $^{208}\text{Pb}/^{204}\text{Pb}$  ratios. Samples with high  $^{40}\text{Ar}/^{36}\text{Ar}$  ratios have typical depleted-mantle  $^{206}\text{Pb}/^{204}\text{Pb}$  ratios; those with low  $^{40}\text{Ar}/^{36}\text{Ar}$  have radiogenic lead (Fig. 1). The curvature of these Ar-Pb isotopic correlations is weak.

These correlations cannot reasonably be attributed, directly or indirectly, to shallow-level contamination by atmospheric argon; this would mean that the samples most contaminated in argon are the most radiogenic in Pb, for which there is no obvious reason. In the case of mixing between two magmas, it is unlikely that the magma with the most radiogenic lead would also be the most degassed (hence the most susceptible to contamination), especially over a span of 20,000 km

Laboratoire de Géochimie et Cosmochimie, Institut de Physique du Globe de Paris (IPGP), 4 place Jussieu, 75252 Paris Cedex 05, France.

\*To whom correspondence should be addressed. Present address: Groupe de Géochimie des Gaz Rares, Département de Sciences de la Terre et U.M.R. Orsayterre, Université Paris 11–Sud, 91405 Orsay Cedex, France.

†Present address: Woods Hole Oceanographic Institution, Marine Chemistry and Geochemistry, Clarke Building, 360 Woods Hole Road, Mail Stop 25, Woods Hole, MA 02543, USA.

‡Present address: Observatoire Volcanologique du Piton de la Fournaise, 14RN3, le 27e Km, 97418 La Plaine des Cafres, La Réunion, France.